Efficient Solar-to-Hydrogen Conversion Efficiency at pH 7 Based on a PV-EC Cell with an Oligomeric Molecular Anode

Yuanyuan Shi,[1,#] Tsung-Yu Hsieh,[1] MD Asmaul Hoque,[1] Werther Cambarau,[1] Stéphanie Narbey,[2] Carolina Gimbert-Suriñach,[1,] Emilio Palomares,[1,3,*] Mario Lanza,[4,*] Antoni Llobet[1,5,*]*

[1] Institute of Chemical Research of Catalonia (ICIQ), Barcelona Institute of Science and Technology (BIST), Avinguda Països Catalans, 16, 43007 Tarragona, Spain

[2] Solaronix S.A., Rue de l'Ouriette 129, Aubonne, CH-1170, Switzerland

[3] ICREA, Passeig Lluís Companys 23, Barcelona, Spain

[4] Physical Sciences and Engineering Division, King Abdullah University of Science and Technology (KAUST), Thuwal 23955-6900, Saudi Arabia

[5] Departament de Química, Universitat Autònoma de Barcelona (UAB), 08193 Cerdanyola del Vallès, Barcelona, Spain

[#] Present address: IMEC, Kapeldreef 75, 3001 Leuven, Belgium

Corresponding Authors

* cgimbert@iciq.cat; epalomares@iciq.es; mario.lanza@kaust.edu.sa; allobet@iciq.cat

Abstract

On the urgent quest for green energy vectors, the generation of hydrogen by water splitting with sunlight occupies a preeminent standpoint. The highest solar-to-hydrogen (STH) efficiencies have been achieved with Photovoltaic-Electrochemical (PV-EC) systems. However, most of the PV-EC water splitting devices need to work at extreme conditions, such as in concentrated solutions of $HClO_4$ or KOH, or under highly concentrated solar illumination. In this work, a molecular catalyst-based anode is incorporated for the first time in a PV-EC configuration, achieving an impressive 21.2% STH efficiency at neutral pH. Moreover, as opposed to metal oxide-based anodes, the molecular catalyst-based anode allows working with extremely small catalyst loadings (< 16 nmol/cm^2) due to a well defined metallic center, which is responsible for the fast catalysis of the reaction in the anodic compartment. This work paves the way of integrating molecular materials in the efficient PV-EC water splitting systems.

TOC graphic

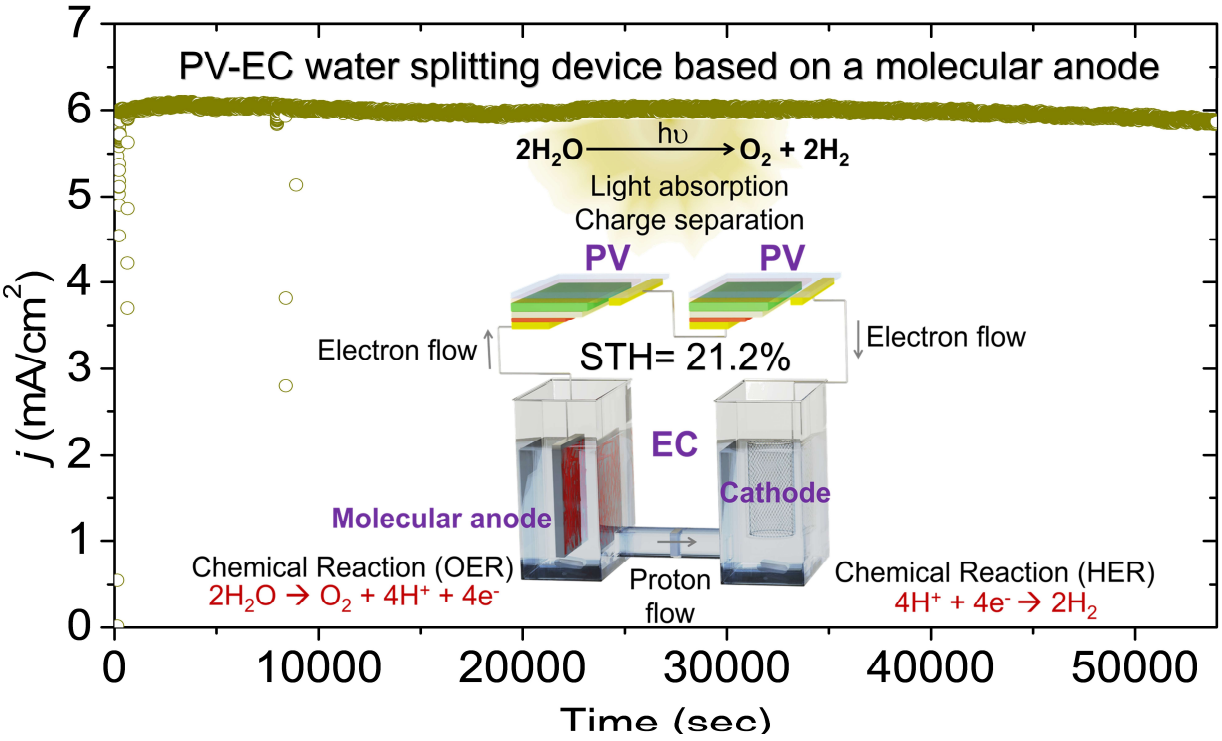
PV-EC water splitting device based on a molecular anode
2H2O hυ O2 + 2H2
Light absorption
Charge separation
PV
PV
Electron flow
STH= 21.2%
Electron flow
EC
Cathode
Molecular anode
Chemical Reaction (OER)
2H2O → O2 + 4H+ + 4e-
Proton flow
Chemical Reaction (HER)
4H+ + 4e- → 2H2
j (mA/cm2)
Time (sec)
0
1
2
3
4
5
6
7
0
10000
20000
30000
40000
50000

Introduction

In the last decades, increasing society awareness about the problems associated with using fossil fuels and the massive generation of CO_2 as a greenhouse gas has fostered the need for developing new energy conversion avenues based on clean and sustainable sources.[1-4] One of the most promising solutions in the short term is water splitting with sunlight (hυ-WS) that generates oxygen and hydrogen as a clean fuel. Furthermore, the use of hydrogen as a fuel in vehicles, as well as its transportation and storage are already technologically established today.[5-9] Efficient hυ-WS requires a combination of compatible components working in a synchronized manner that should be mastered so that it carries out the corresponding independent steps involved in this complex process. The first step involves light absorption and charge separation, which generates an excited state that will drive the reductive and oxidative chemical reactions. The chemical reactions are typically the slowest processes and thus it is a crucial issue to develop fast, rugged and efficient catalysts that can carry them out at low overpotentials.[10, 11] One of the devices that can be used to achieve hυ-WS is the so-called Photovoltaics coupled to Electrochemical Cells (PV-EC),[12,13] where the light absorption and charge separation is achieved with a photovoltaic cell that is coupled via a wire to the anode and cathode of an electrochemical cell (Figure 1). In this arrangement the PV is isolated from the aqueous medium, often incompatible with currently available efficient light absorbers while the anode and cathode contain efficient catalysts that ensure sufficiently fast chemical reactions. The catalysts can be either dissolved in the corresponding anodic and cathodic compartment or attached at the surface of the electrodes. The latter is normally preferred from an engineering perspective because it significantly simplifies the complexity of the device, which can be conceived in a modular manner. Further, the modular approach allows to optimize each component independently.

A suitable power output of the PV cell is required to achieve the overpotential needed to drive the chemical reactions in the EC. The latter will require a minimum of 1.23 V, dictated by the thermodynamics of the WS reaction and an additional voltage, which will depend on the activation energies of the chemical reactions in the electrolyzer.[8,14,15] This overpotential is dictated by the nature of the catalysts and is thus one of the crucial elements of the PV-EC device; the lower the working overpotential, the more efficient the device will be. Further, a fast catalyst working at lower overpotentials will enhance its stability during the working conditions. The performance of the catalyst is critical for the long-term stability of the whole device. Its performance will depend not only on the intrinsic nature of the catalyst but also on the stability of electrode-catalyst interface which in turn will also be a function of pH. The latter is another important parameter that needs to be taken into consideration. Ideally the pH of the EC should operate close to 7 since it minimizes the corrosion and solubilization effects that occur at extreme pHs. It further minimizes operation costs and simplifies installation specially in remote locations where specific chemicals might be difficult to obtain and correctly dispose.

Unfortunately, most of the catalysts used in PV-EC systems are based on metal oxides such as iron, nickel or cobalt oxides that are stable only under extreme conditions typically in concentrated solutions of $HClO_4$ or KOH[16] and thus most of the devices reported so far had no other choice but to work under these drastic conditions. Nevertheless, at these extreme pHs, related PV-EC devices containing Group III-V[17-20] absorbers give STH efficiencies up to an impressive 20%, CIGS[21] and Si[22-28] reach values close to 17% and perovskite or organic solar cells at about 12.3% and 6 %, respectively.[29-34] At neutral or close to neutral pH good performance and high STH efficiencies are only achieved using platinum or iridium based catalysts and under high values of simulated solar flux irradiation[35] or under concentrated solar type of conditions.[36-38] Using this strategy record STH efficiencies up to 30% have been achieved with InGaP/GaAs/Ge absorber at 42 suns.[38] Under mild

conditions at pH 7 and 1 sun, only two examples are reported that use InGaP/GaAs/Ge[39] as absorber and reaches STH of 17.9% or a compact triple junction polymer solar cell with STH of 6%.[40] Overall, the efficiencies achieved using PV-EC configurations are significantly higher than those obtained through other strategies such as direct one-pot photocatalysis[13, 41] or systems combining photoelectrochemical and photovoltaic technologies (PEC-PV)[42] with 2% and 8.1% record efficiencies, respectively.

One of the challenges currently hindering the implementation of PV-EC devices is to find systems that work in mild conditions such as pH 7 and 1 sun or lower irradiation intensities, over prolonged reaction times without any loss of activity. It is thus imperative to use highly performing catalysts for water oxidation and water reduction at pH 7 as well as absorbers that can generate the needed potential and that are stable for long periods of time.

We have recently described extremely robust and an efficient molecular Ru water oxidation catalyst (WOC) [Ru(O)(tda)(py)$_2$] (where tda = [2,2':6',2''-terpyridine]-6,6''-dicarboxylato and py = pyridine) that works at pH 7,[43] and carries out more than a million turnovers without any sign of deactivation when properly functionalized and anchored on a conductive support.[44] Further, we have also shown that it can reach turnover frequencies over 7,700s^{-1} that are about 10^5 times better than most of the reported WOCs based on oxides.[45] Recently we have shown that oligomeric Ru-tda derivates of general formula [Ru(O)(tda)(4.4'-bpy)$_2$]n (where bpy = 4,4'-bipyridine), have even better performances at pH 7.[46]

Given the unprecedented performance of these molecular WOCs at pH 7, we for the first time succeed to anchor them on graphitic surfaces to generate stable molecular anodes and couple them to absorbers based on both lab-fabricated and commercially available solar cells (including perovskite and InGaP/GaAs/Ge) in PV-EC configurations. Our molecular anode is compatible to different types of PV cells based PV-EC system. Here on we report a molecular anode-based PV-

EC cells with unprecedented performance in terms of STH efficiency (21.2%) and long term stability (> 15 hours) at pH 7, containing an extremely small amount (< 16 nmol/cm^2) of a molecular catalyst and with no other external input than sunlight.

Experimental Procedures and Methods

Synthesis of oligomeric ruthenium molecular complex RuPol with chemical formula {Ru^{II}(tda)(bipy)}$_{15}$ (where tda = [2,2':6',2''-terpyridine]-6,6''-dicarboxylato and bipy = 4,4'-bipyridine): The synthesis of the oligomer follows a reported procedure,[46] based on the synthesis used for the original complex [Ru^{II}(tda)(py)$_2$] (where py = pyridine) by substituting pyridine by 4,4'-bipyridine bridging ligand.[43] The final compound has been found to contain 15 units of the {Ru^{II}(tda)(bipy)} metallic centers. The chemical structure of the ruthenium molecular catalyst RuPol is shown in Figure S1 (Supporting Information).

Preparation of the anodes containing the RuPol material: Two kinds of RuPol molecular anodes were prepared, depending on the conductive substrate where the catalyst is deposited. The first kind consists of conductive FTO coated glass from XopFisica (thickness, 2.3-3.0 mm; resistance, 6-9 Ω/cm^2) and the second kind consists of glassy carbon plate from HTW® (20 mm x 10 mm x 180 mm) substrates. Before loading the water oxidation catalyst on the surface of the substrates, the FTO coated glass is cleaned with an alkaline solution ($V_{HELLMANEX}$: $V_{Milli\text{-}Q\ water}$ =100:1, Hellmanex from Hellma GmbH & CO. KG), Milli-Q water and ethanol. Each cleaning step are under 10 min sonication and then rinsed by the corresponding solvents. After all these steps, the FTO coated glass is dried in the oven at 100 ℃ overnight, and then annealed at 300 ℃ for 30 min in the furnace to remove the organic contaminations on the surface and ensure a good conductivity. The carbon plates are just rinsed with Milli-Q water and dried with fiber-free wipers. After cleaning these substrates, 10 mg of multi wall carbon nanotubes (MWCNTs, Nanostructured & Amorphous

Materials, Inc.) powders are suspended in 10 mL of Tetrahydrofuran (THF, dried, purity ⩾ 99%, Sigma-Aldrich) under 40 min sonication. Then this CNTs suspension is used to cover the surface of ~1.87 cm^2 cleaned FTO glass and ~1.5 cm^2 carbon plates by drop casting with 15 drops (20 µL per drop), each drop is placed after the last drop is totally dried. Then 4.3 mg of RuPol powder are dissolved in 5 mL of 2,2,2-Trifluoroethanol (TFE, Sigma-Aldrich). Finally, the RuPol solution is drop casted on the CNTs covered FTO glass and carbon plates (3 drops, 20 µL per drop), new drops are added only after the last drop is totally dried on the substrate. The resulting anodes are indicated as RuPol@CNTs@FTO and RuPol@CNTs@C-plate, respectively. A schematic describing the whole preparation process on FTO coated glass is given in Figure S2 (Supporting Information).

Morphology characterization of the molecular anode RuPol@CNTs@FTO: The surface of the RuPol@CNTs@FTO electrodes have been characterized by scanning electron microscopy (SEM, JEOL JSM-6400 model) from both cross-sectional and top views (Figure S3, Supporting Information). For the cross-sectional view characterization, the prepared electrodes were cleaved carefully, and the fresh edges were used for the analysis.

Electrochemical characterization of the molecular anode RuPol@CNTs@FTO: All electrochemical experiments were performed by using CHI 660D and CHI 620E potentiostats (CH Instruments, Inc.). Two phosphate based supporting electrolytes were used for the electrochemical test, which are a pH 7 buffer made of 9.785 g NaH_2PO_4 and 19.945 g Na_2HPO_4 (ionic strength: 1 M) and a pH 12 buffer made of 0.5187 g $NaHPO_4$ and 1.033 g Na_3PO_4 (ionic strength: 0.1 M). The pH values of the buffer electrolytes were measured by a pH meter (Mettler toledo, Inc.). In three electrode configuration system, all the electrochemical experiments were done in a one compartment cell (25 mL volume) with the RuPol@CNTs@FTO or RuPol@CNTs@C-plate as working electrode, Pt mesh as counter electrode and Hg/Hg_2SO_4 (saturated K_2SO_4) as reference electrode. However, in the two-electrode configuration, all the measurements were performed in a

two-compartments cell (10 mL per compartment) with a separation frit, and without using any reference electrode (the working lead connects with the RuPol@CNTs@FTO or RuPol@CNTs@C-plate, and the auxiliary lead is connected together with the reference lead to the Pt mesh). All the cyclic voltammetries (CVs), chronopotentiometry and constant potential electrolysis were collected in three-electrode configuration. The CVs were recorded with *i*R compensation and at a scan rate of 100 mV/s, while chronopotentiometry and constant potential electrolysis were obtained without *i*R compensation. All the linear sweep voltammetry experiments (LSVs) were collected in two-electrode configuration without *i*R compensation and at a scan rate of 10 mV/s. When the electrodes were placed inside the sealed two-compartment cell, the electrolyte was degassed with N_2 for 15-20 min prior to the LSV measurements. The loading of the ruthenium molecular catalyst Γ (mol/cm^2) on the substrate can be calculated by the averaged charge (Q_{Ru}) under the $Ru^{III/II}$ and $Ru^{IV/III}$ oxidation waves in the second CV scan (the first CV is always unstable) of the anodes, with the formula $\Gamma(mol/cm^2)= Q_{Ru}/(A\times F)$. A is the geometrical area of the RuPol@CNTs@FTO or RuPol@CNTs@C-plate electrode and F is the Faradaic constant. According to this calculation, the loadings of the ruthenium molecular catalyst in RuPol@CNTs@FTO (1.8-1.87 cm^2) and RuPol@CNTs@C-plate (1.5 cm^2) are 16 nmol/cm^2 and 6.2 nmol/cm^2, respectively.

Fabrication of perovskite solar cells: Fluoride-doped tin oxide (FTO) substrates were patterned in a chemical way using zinc powder and 5 M hydrochloride acid solution. The patterned substrates were then ultrasonically cleaned in i) 2% Hellmanex detergent and ii) deionised water for 30 min. The substrates were exposed to UV-ozone environment for 10 min before use. A thin titanium dioxide (TiO_2) film was deposited on a cleaned FTO substrate by spin coating a solution that was composed of 0.3 M titanium diisopropoxide bis(acetylacetonate) (Sigma-Aldrich, 75wt% in isopropanol) diluted in isopropanol (IPA) at 4000 rpm for 30 s. The substrate was heated on a

hotplate at 120°C for 5 min followed by sintering at 450°C for 30 min. After slowly cooling down to room temperature, the substrate was immersed into a 40 mM titanium tetrachloride solution (Sigma-Aldrich, 90mM, diluted in deionized water) at 70°C for 30 min. After mildly rinsing with i) deionized water and ii) ethanol, the substrate was dried by airflow. A mesoporous TiO_2 layer was deposited using a diluted TiO_2 paste (30 nm in particle size, dyesol) in a ratio of paste/ethanol, 1/7 (w/w) at 6000 rpm for 30 s. Then, the substrate was heated on a hotplate at 120°C for 5 min and followed by a calcination at 500°C for 30 min. 1.2 M lead iodide (PbI_2) solution was prepared by dissolving PbI_2 powder (Alfa Aeser, 99.9985%) in a blend of dimethylformamide (DMF, Sigma-Aldrich, anhydrous) and dimethyl sulfoxide (DMSO, Sigma-Aldrich, ACS reagent grade) at a volume ratio of 9/1. The perovskite layer was prepared by means of two-step spin-coating process. Firstly, the PbI_2 solution (kept at 70°C during whole process) was spin coated on the previously prepared mesoporous layer at 3000 rpm for 30 s in dynamic way. Secondly, 100 μL of an organic solutioncomposed of 195 mM methylammonium iodide (MAI), 55 mM formamidinium iodide (FAI), 28 mM methylammonium bromine (MABr) and 70 mM methylammonium chloride (MACl) in IPA, was dropped on the PbI_2 coated substrate by spin coating at 2000 rpm for 30 s. The as prepared perovskite film was heated on a hotplate at 120°C for 20 min. After cooling down to room temperature, a layer of hole transporting material was spin coated on the top using a solution, composed of 60 mM 2,2',7,7'- Tetrakis-(N,N-di-4-methoxyphenylamino)-9,9'-spirobifluorene (spiro-OMeTAD, 1-Material), 32 mM lithium bis(trifluoromethylsulphonyl)imide (Li-TFSI, Sigma-Aldrich), and 195 mM tert-butylpyridine (tBP, Sigma-Aldrich, 96%) in chlorobenzene (Sigma-Aldrich, anhydrous, 99.8%) at 4000 rpm for 30 s. Finally, a gold layer of 80-nm thickness was thermal evaporated on the top as a terminal electrode. The entire fabrication process was conducted in a glove box with both moisture and oxygen controlled.

Measurements of perovskite solar cells: The current-voltage response of new devices was measured under a Sun 2000 solar simulator (150 W, ABET Technologies) equipped with a Keithley 2400 digital source meter. The illumination intensity was calibrated using a commercial silicon photodiode at 1 sun (100 mW/cm^2). No bias or illumination was pre-treated on devices in every measurement. During the scan, the scan step, integration time and delay time were set at 10 mV, 3 ms and 50 ms, respectively, which corresponded to a scan rate of 42.9 mV/s. Neutral-density (ND) filters were applied as measurements under different light intensities.

PV-EC solar-driven water splitting: All the experiments were performed in a two-compartment, and two-electrode configuration. The two-compartments cell is filled with 6 mL phosphate buffer (pH 7, 1 M) at each compartment, and the electrolyte was also degassed with N_2 flow for 10-20 min after placing the anodes and cathodes. The photocurrent generated during the light driven PV-EC water splitting experiment was monitored with a CHI 620E potentiostat by performing a bulk electrolysis at 0 V bias, which works as an ammeter in this case. A schematic and digital photograph of the setup is shown in Figure S7 (Supporting Information). As it is shown Figure S7 (Supporting Information), the PV cells are illuminated by a 150 W Xenon lamp (LS-150, ABET technology) equipped with a filter to block UV light ($\lambda < 400$ nm). The light intensity can be measured by using a calibrated silicon photodiode at 25 °C, and the illumination reaching the PV cells is tuned by using different ND filters depending on the desired current. In the case of our fabricated perovskite cells (0.18 cm^2) and commercial perovskite solar cells (0.5 cm^2, from Solaronix, https://www.solaronix.com/news/solaronix-achieves-major-breakthrough-toward-perovskite-solar-cell-industrialization/), the light intensity was set to 0.28-0.29 sun. 0.35-0.36 sun light intensity was used to illuminate the InGaP/GaAs/Ge triple junction solar cell (0.18 cm^2, purchased from Fullsuns Energy Technology Co., Ltd). Two metallic meshes were also used to obtain a large and uniform illumination. The cathode side of the PV cells was connected with the working lead

of the potentiostat, while the reference and auxiliary leads are connected together to the cathode of the electrolyzer. Finally, an additional electrical wire was needed to connect the anode side of the PV cells to the anode of the electrolyzer. The resistance of this configuration was measured before starting the illumination, which was in the range of 210-240 Ω. Once we turned on the light, the spontaneous water splitting was triggered. During the process the generated photocurrent was monitored through the potentiostat while the generated oxygen (O_2) and hydrogen (H_2) gases were monitored through an O_2 sensitive OX-NP15127 Clark electrode (Unisense) and a H_2 sensitive H2-NP706731 Clark electrode (Unisense), respectively.

Results and Discussion

Molecular anode for water oxidation

We have recently described the synthesis of a coordination oligomer that is a catalyst precursor of a highly active water oxidation catalyst and that has a high affinity to graphitic surfaces such as multiwall carbon nanotubes.[46] The structure of its precursor is defined as $\{Ru^{II}(tda)(bpy)\}_{15}$ (RuPol) and represents an evolution of a mononuclear catalyst precursor that has shown excellent catalytic performance in homogeneous[37] and in heterogeneous[44, 47-48] phase. Both mononuclear complex and oligomer show identical electrochemistry due to the analogous octahedral coordination sphere of the ruthenium centers at oxidation state +2, composed of five pyridine donors and one carboxylate ligand (Figure S1). The length of the oligomeric material has been ascertained by means of ^{1}H NMR spectroscopy and scanning tunneling microscopy (STM).[46]

The oligomer RuPol was prepared following a reported methodology and isolated as a red-brown powder,[46] which was dissolved in trifluoroethanol and carefully drop cast on top of a FTO electrode covered with carbon nanotubes (CNTs) to give the electrode RuPol@MWCNTs@FTO (functionalized surface = 1 × 2 cm^2, Figure S2-S3, Supporting Information). A cross sectional

scanning electron microscopy (SEM) image shows that the thickness of the RuPol@CNTs is around 50 μm and analysis of the chemical composition of the surface by the energy-dispersive X-ray spectroscopy (EDX) confirms the presence of the ruthenium (Figure S3, Supporting Information).

A cyclic voltammetry experiment of this hybrid electrode shows the typical $Ru^{III/II}$ and $Ru^{IV/III}$ redox couples that characterize the catalyst precursor (Figure 2, dashed black trace).[43] The loading of the electroactive complex on the surface is 16 nmol/cm^2, a similar value to that of analogous electrodes using glassy carbon as conductive substrate and one of the highest loadings reported for molecular anodes in general.[44, 47-49] When the electrode RuPol@MWCNTs@FTO is subjected to a bulk electrolysis at E_{app} = 1.25 V vs. NHE at pH 12, the precursor is converted to the active catalyst characterized by a Ru-OH_2 fragment, which is the result of the coordination of a water molecule upon oxidation and that allows for proton coupled electron transfer processes leading to high valent seven coordinated Ru-OH/ Ru=O species responsible to trigger the catalysis (Figure S1).[43-44,46] The active oligomer shows a couple of reversible waves that are anodically shifted as compared to the precursor (Figure 2, compare red and dashed black traces). In addition, a high catalytic current due to the oxidation of water to dioxygen appears at $E_{cat,onset} \approx$ 1.15 V vs. NHE at pH 7. The catalytic performance of the active electrode, Ru(O)Pol@MWCNTs@FTO, was tested in a two-compartment electrochemical cell at pH 7 using a platinum mesh as counter electrode, showing no loss of activity after 12 h of experiment (Figure S4-S5, Supporting Information).

The sharp slope for the catalytic process by Ru(O)Pol@MWCNTs@FTO in the voltammetry experiment in Figure 2 is responsible for the high performance of this anode, showing working voltages as low as 1.15 V vs. NHE and 1.27 V vs. NHE for relevant current outputs of 0.56 mA and 1 mA respectively at pH 7 (Figure S5, Supporting Information). In sharp contrast, an analogous electrode based on ruthenium oxide, RuO_2@CNTs@FTO, with similar $E_{cat,onset} \approx$ 1.10 V vs. NHE,

requires higher potentials to achieve the same current density as evidenced in cyclic voltammetry and chronopotentiometry experiments of Figure S6 (Supporting Information). Therefore, to achieve high currents, the loading of expensive ruthenium metal in RuO_2 based anodes is often orders of magnitude higher than that required in the Ru(O)Pol@MWCNTs@FTO electrode reported here.[16, 50-51] The oligomeric structure of the molecular material Ru(O)Pol provides unprecedented stability for molecular type of catalysts under oxidation conditions at high potentials and allows us to use mild conditions such as pH 7 phosphate buffer, incompatible with common electrolyzers.

State-of-the-art perovskite solar cell for water splitting

State of the art perovskite solar cells can provide open circuit voltages (V_{OC}) around 1.1 V.[52] Since the water splitting reaction requires a minimum working potential of 1.5-1.8 V accounting for the thermodynamics of the reaction and the kinetic barrier of the electrolyzer, at least two perovskite solar cells need to be connected in series.[8, 14, 15, 29] Figure 3 shows the architecture of our fabricated perovskite solar cells and the *J-V* curve of two devices connected in series, generating an effective illumination area of 0.18 cm^2. The V_{OC} of the resulting device is larger than 2 V, and the maximum power point ranges between 1.75-1.85 V depending on the light intensity. Indeed, it is well above the required potential for the hυ-WS reaction. The solar-to-electric power conversion efficiencies (PCE) and fill factors (FF) are around 18 % and 72-75 %, respectively (Table S1, Supporting Information). These values are comparable to standard perovskite solar cells and therefore are excellent candidates to be integrated in PV-EC.

PV-EC with perovskite solar cells

The PV-EC device was assembled by coupling the two-series connected perovskite PV cells with the electrolyzer composed of Ru(O)Pol@CNTs@FTO anode and platinum mesh cathode at pH 7 as shown in Figure 1 and Figure S7 (Supporting Information). The overlapping of the *J-V* curves

of the 2 PVs and that of the EC shows a match point at a working voltage of E = 1.63 V and a current density of j = 3.1 mA/cm^2 (Figure 4a). In this study, we explore the use of low light intensity (0.28 sun illumination) given the benefits it can give to countries with low sunlight radiation. Unlike silicon solar cells, perovskite solar cells show greater efficiencies at low light illumination due to their working principles that lead to high V_{OC} even at light intensities lower than 1 sun (100 mW/cm^2@1.5AM G).[53]

The evolution of the current density over a 4 h time slot for a typical measurement is given in Figure 4b. It shows a fairly stable current density of j ~ 3 mA/cm^2 and manually collected working voltages in the range of 1.60-1.64 V (Table S2, Supporting Information), which perfectly match the *J-V* curve overlapping point. Experimentally, the system shows higher stability when chopped light is employed, a phenomenon that has been attributed to the ions mobility within the perovskite structure that leads to hysteresis on the photocurrent vs. voltage measurements. By constantly shutting down the light, we allow for the control of the ion mobility and, thus, the device voltage remains fairly constant. It is important to remark that a noticeable change in performance of the 2 PV assembly is observed after the four hours run. Yet, the cyclic voltammetry analysis of the molecular anode after the experiment shows that the electrode maintains full catalytic activity towards the oxygen evolution reaction and that the molecular nature of the electrode is intact (Figure S8, Supporting Information).

The oxygen and hydrogen generated during the water splitting experiment were measured with a Clark electrode accounting for a Faradaic efficiency close to 100 % (Figure S8, Supporting Information). With these data, a remarkable solar-to-hydrogen efficiency of ~13.2 % is calculated through *Equation 1*, where η_F is the Faradaic efficiency calculated from the gas evolution, j_{OP} is the operating current density of the solar-driven PV-EC water splitting reaction, and P_{in} is the solar intensity of the illumination, which is 28 mW/cm^2 in our experiment. This value is among the best

PV-EC systems that use PV that do not contain Group III-V elements (Table S4, Supporting Information) including those based on perovskite solar cells.[2] Note also that our working pH is 7.

$$STH = \frac{1.23\ (V) \times \eta_F \times j_{op}\ (mA/cm^2)}{P_{in}\ (mW/cm^2)} \qquad (Equation\ 1)$$

We have extended the use of the molecular anode Ru(O)Pol@CNTs@FTO to PV-EC devices made of commercially available perovskite solar cells (Figure S9, Supporting Information). Although the matching point displayed by the overlapping of the *J-V* curves is beyond the maximum power point, we can observe that the device keeps 93 % and 74 % stability after 2 and 20 hours, respectively with no-chopped light employed. Importantly, after 20 hours PV-EC hυ-WS reaction, the activity of the Ru(O)Pol@CNTs@FTO electrode is unaltered. On the other hand, commercial perovskite solar cells show some degradation, induced by the mismatch of the working current/voltage of the PV-EC water splitting device and the maximum power point of the solar cells. Those devices did not need the light chopped sources due to the minor hysteresis of their I-V curves. Even though the stability of the perovskite solar cells has been dramatically improved during the past decade, they are still the limiting factor in terms of overall performance of the present PV-EC device described here.

PV-EC with III-V group solar cell

We turn now on the use of a commercially available InGaP/GaAs/Ge triple junction solar cell (TJSC) together with our Ru(O)Pol@CNTs@FTO electrode. Figure 5a shows the *J-V* characteristics of the PV under illumination overlapped with the *j-E* curve of an electrolyzer made of the Ru(O)Pol@CNTs@FTO anode and Pt mesh cathode at pH 7. The TJSC shows an open circuit potential of V_{OC} = 2.37 V and short circuit current of j_{SC} = 6.2 mA/cm^2, while the match

point between PV and EC lies at E = 1.85 V and j = 6.0 mA/cm^2. These values match the working conditions of the assembled PV-EC device as shown in the j/t plot of Figure 5b that performs with a working potential E = 1.85-1.90 V and j = 6.0 mA/cm^2. As expected, the device shows no degradation of the PV and, moreover, the Ru(O)Pol@CNTs@FTO anode remains without any sign of degradation after 15 hours of irradiation performing the water oxidation reaction (Figure 5c-d), manifesting again the high stability of the molecular anode. The key features that allow us to confirm that the catalyst is intact are the two pH-dependent redox waves observed in the cyclic voltammetry in Figure 5d, that correspond to the Ru^{II}-OH_2 to Ru^{III}-OH and Ru^{III}-OH to Ru^{IV}=O species. The latter, undergoes a last oxidation to Ru^{V}=O, which is the active intermediate reacting with a water molecule in the key step, when the O-O bond forms to produce O_2 gas.[45, 54] It is the nature of the molecular active site of the catalyst that gives such a fast catalysis leading to very sharp slopes and thus allowing to reach high currents at potentials very close to the onset (Figure 5d, grey area) with overpotentials as low as 350 mV in the best case. It is also important to realize here, that the amount of catalyst loaded at the surface of the nanotubes is in the range of 20 nmol of Ru per cm^2, that is orders of magnitude lower than what is generally used for the case of oxides used as water oxidation catalysts.[16, 50-51] Remarkably the high performance and stability of the hybrid electrode Ru(O)Pol@CNTs@FTO in the PV-EC device is maintained also on conductive graphitic supports such as carbon plates as shown in the Figure S11 (Supporting Information).

Gas measurements allowed us to calculate a Faradaic efficiency close to 100 % for both oxygen and hydrogen (Figure S10, Supporting Information) and a record high STH of 21.2 % at pH 7 and room temperature. This is the highest value reported in the scientific literature without using a concentrated light illumination system (Table S4, Supporting Information).

Summary and Conclusions

In summary, a highly active oligomeric molecular anode Ru(O)Pol@CNTs@FTO for the oxidation of water to dioxygen has been prepared and successfully incorporated into a PV-EC device with outstanding performance in the conversion of water into hydrogen and oxygen by using sunlight as the only input of energy. The Ru(O)Pol molecule is made of a coordination oligomer, which contains a well defined ruthenium center that is responsible for the fast catalysis of the reaction in the anodic compartment. Moreover, it allows working at voltages very close to the onset of the catalytic process with extremely small catalyst loadings. The integration of the Ru(O)Pol@CNTs@FTO molecular anode has been done in combination with either lab-fabricated perovskite solar cells achieving STH of 13.2 %, or a commercially available InGaP/GaAs/Ge triple junction solar cell with a record high STH = 21.2 % both at room temperature and pH 7. Remarkably, the Ru(O)Pol@CNTs@FTO molecular anode is highly stable showing no appreciable degradation after working times beyond 15 hours. Furthermore, because of the modular approach used here, a graphitic carbon plate can also be used as conducting support instead of FTO, highlighting the high versatility of this device where all the components can be individually improved and later ensembled. Overall, our study paves the way of novel promising molecular anodes for the water oxidation reaction, their role in the development of PV-EC solar-driven water splitting devices and their application in future fully integrated artificial photosynthetic systems.

ASSOCIATED CONTENT

Supporting Information

The Supporting Information is available free of charge at https://pubs.acs.org

Additional experimental results and data (Figures S1− S11 and Table S1-S4).

AUTHOR INFORMATION

Corresponding Authors

Carolina Gimbert-Suriñach - Institute of Chemical Research of Catalonia (ICIQ), Barcelona Institute of Science and Technology (BIST), Avinguda Països Catalans, 16, 43007 Tarragona, Spain; Emial: cgimbert@iciq.cat

ORCID: 0000-0002-4412-7607

Emilio Palomares - Institute of Chemical Research of Catalonia (ICIQ), Barcelona Institute of Science and Technology (BIST), Avinguda Països Catalans, 16, 43007 Tarragona, Spain; ICREA, Passeig Lluís Companys 23, Barcelona, Spain; Email: epalomares@iciq.es

ORCID: 0000-0002-5092-9227

Mario Lanza - Physical Sciences and Engineering Division, King Abdullah University of Science and Technology (KAUST), Thuwal 23955-6900, Saudi Arabia; Email: mario.lanza@kaust.edu.sa

ORCID: 0000-0003-4756-8632

Antoni Llobet - Institute of Chemical Research of Catalonia (ICIQ), Barcelona Institute of Science and Technology (BIST), Avinguda Països Catalans, 16, 43007 Tarragona, Spain; Departament de Química, Universitat Autònoma de Barcelona (UAB), 08193 Cerdanyola del Vallès, Barcelona, Spain; Email: allobet@iciq.cat

ORCID: 0000-0002-6176-5272

Authors

Yuanyuan Shi - Institute of Functional Nano and Soft Materials (FUNSOM), Collaborative Innovation Center of Suzhou Nanoscience & Technology, Soochow University, 215123 Suzhou, China; Institute of Chemical Research of Catalonia (ICIQ), Barcelona Institute of Science and Technology (BIST), Avinguda Països Catalans, 16, 43007 Tarragona, Spain

ORCID: 0000-0002-4836-6752

Tsung-Yu Hsieh - Institute of Chemical Research of Catalonia (ICIQ), Barcelona Institute of Science and Technology (BIST), Avinguda Països Catalans, 16, 43007 Tarragona, Spain

MD Asmaul Hoque - Institute of Chemical Research of Catalonia (ICIQ), Barcelona Institute of Science and Technology (BIST), Avinguda Països Catalans, 16, 43007 Tarragona, Spain

Werther Cambarau - Institute of Chemical Research of Catalonia (ICIQ), Barcelona Institute of Science and Technology (BIST), Avinguda Països Catalans, 16, 43007 Tarragona, Spain

Stéphanie Narbey - Solaronix S.A., Rue de l'Ouriette 129, Aubonne, CH-1170, Switzerland

Notes

The authors declare no competing financial interest.

ACKNOWLEDGMENT

This work has been supported by the Young 1000 Global Talent Recruitment Program of the Ministry of Education of China, the National Natural Science Foundation of China (grants no. 61502326, 41550110223, 11661131002), the Jiangsu Government (grant no. BK20150343), the Ministry of Finance of China (grant no. SX21400213). The Collaborative Innovation Center of Suzhou Nano Science & Technology, the Jiangsu Key Laboratory for Carbon-Based Functional Materials & Devices and the Priority Academic Program Development of Jiangsu Higher Education Institutions are also acknowledged. MINECO and FEDER (PID2019-111617RB-I00), EU-funded ITN eSCALED (Grant agreement ID: 765376) and AGAUR (2017-SGR-1631), are also gratefully acknowledged for providing financial support. Shaochuan Chen from RWTH Aachen University is acknowledged for drawing some of the 3D images.

References

References

(1) Vesborg, P. C. K.; Jaramillo, T. F. Addressing the Terawatt Challenge: Scalability in the Supply of Chemical Elements for Renewable Energy. *RSC Adv.* **2012**, *2* (21), 7933–7947.

(2) Perera, F. Pollution from Fossil-Fuel Combustion Is the Leading Environmental Threat to Global Pediatric Health and Equity: Solutions Exist. *Int. J. Environ. Res. Public Health* **2017**, *15* (1), 16.

(3) Lewis, N. S.; Nocera, D. G. Powering the Planet: Chemical Challenges in Solar Energy Utilization. *Proc. Natl. Acad. Sci.* **2006**, *103* (43), 15729–15735.

(4) Armaroli, N.; Balzani, V. The Future of Energy Supply: Challenges and Opportunities. *Angew. Chem.- Int. Ed.* **2007**, *46* (1–2), 52–66.

(5) Abbasi, T.; Abbasi, S. A. 'Renewable' Hydrogen: Prospects and Challenges. *Sustainable Energy Rev.* **2011**, *15* (6), 3034–3040.

(6) Balat, M. Potential Importance of Hydrogen as a Future Solution to Environmental and Transportation Problems. *Inter. J. of Hydrogen Energy* **2008**, *33* (15), 4013–4029.

(7) Turner, J.; Sverdrup, G.; Mann, M. K.; Maness, P.-C.; Kroposki, B.; Ghirardi, M.; Evans, R. J.; Blake, D. Renewable Hydrogen Production. *Inter. J. of Hydrogen Energy* **2008**, *32* (5), 379–407.

(8) Walter, M. G.; Warren, E. L.; McKone, J. R.; Boettcher, S. W.; Mi, Q.; Santori, E. A.; Lewis, N. S. Solar Water Splitting Cells. *Chem. Rev.* **2010**, *110* (11), 6446–6473.

(9) Bozoglan, E.; Midilli, A.; Hepbasli, A. Sustainable Assessment of Solar Hydrogen Production Techniques. *Energy* **2012**, *46* (1), 85–93.

(10) Francàs, L.; Matheu, R.; Pastor, E.; Reynal, A.; Berardi, S.; Sala, X.; Llobet, A.; Durrant, J. R. Kinetic Analysis of an Efficient Molecular Light-Driven Water Oxidation System. *ACS Catal.* **2017**, *7* (8), 5142–5150.

(11) Berardi, S.; Francàs, L.; Neudeck, S.; Maji, S.; Benet-Buchholz, J.; Meyer, F.; Llobet, A. Efficient Light-Driven Water Oxidation Catalysis by Dinuclear Ruthenium Complexes. *ChemSusChem* **2015**, *8* (21), 3688–3696.

(12) McKone, J. R.; Lewis, N. S.; Gray, H. B. Will Solar-Driven Water-Splitting Devices See the Light of Day? *Chemistry of Materials* **2014**, *26* (1), 407–414.

(13) Ager, J. W.; Shaner, M. R.; Walczak, K. A.; Sharp, I. D.; Ardo, S. Experimental Demonstrations of Spontaneous, Solar-Driven Photoelectrochemical Water Splitting. *Energy Environ. Sci.* **2015**, *8* (10), 2811–2824.

(14) Montoya, J. H.; Seitz, L. C.; Chakthranont, P.; Vojvodic, A.; Jaramillo, T. F.; Nørskov, J. K. Materials for Solar Fuels and Chemicals. *Nat. Mater.* **2017**, *16* (1), 70–81.

(15) Bak, T.; Nowotny, J.; Rekas, M.; Sorrell, C. C. Photo-Electrochemical Hydrogen Generation from Water Using Solar Energy. Materials-Related Aspects. *Inter. J. Hydrogen Energy* **2002**, *27* (10), 991–1022.

(16) McCrory, C. C. L.; Jung, S.; Ferrer, I. M.; Chatman, S. M.; Peters, J. C.; Jaramillo, T. F. Benchmarking Hydrogen Evolving Reaction and Oxygen Evolving Reaction Electrocatalysts for Solar Water Splitting Devices. *J. Am. Chem. Soc.* **2015**, *137* (13), 4347–4357.

(17) Licht, S.; Wang, B.; Mukerji, S.; Soga, T.; Umeno, M.; Tributsch, H. Efficient Solar Water Splitting, Exemplified by RuO_2 -Catalyzed AlGaAs/Si Photoelectrolysis. *The J. Phys. Chem. B* **2000**, *104* (38), 8920–8924.

(18) Khaselev, O. High-Efficiency Integrated Multijunction Photovoltaic/Electrolysis Systems for Hydrogen Production. *Inter. J. Hydrogen Energy* **2001**, *26* (2), 127–132.

(19) Chang, W. J.; Lee, K.-H.; Ha, H.; Jin, K.; Kim, G.; Hwang, S.-T.; Lee, H.; Ahn, S.-W.; Yoon, W.; Seo, H.; Hong, J. S.; Go, Y. K.; Ha, J.-I.; Nam, K. T. Design Principle and Loss Engineering for Photovoltaic–Electrolysis Cell System. *ACS Omega* **2017**, *2* (3), 1009–1018.

(20) Gong, M.; Zhou, W.; Kenney, M. J.; Kapusta, R.; Cowley, S.; Wu, Y.; Lu, B.; Lin, M.-C.; Wang, D.-Y.; Yang, J.; Hwang, B.-J.; Dai, H. Blending Cr_2O_3 into a NiO-Ni Electrocatalyst for Sustained Water Splitting. *Angew. Chem.- Int. Ed.* **2015**, *54* (41), 11989–11993.

(21) Jacobsson, T. J.; Fjällström, V.; Sahlberg, M.; Edoff, M.; Edvinsson, T. A Monolithic Device for Solar Water Splitting Based on Series Interconnected Thin Film Absorbers Reaching over 10% Solar-to-Hydrogen Efficiency. *Energy Environ. Sci.* **2013**, *6* (12), 3676–3683.

(22) Kuang, Y.; Kenney, M. J.; Meng, Y.; Hung, W.-H.; Liu, Y.; Huang, J. E.; Prasanna, R.; Li, P.; Li, Y.; Wang, L.; Lin, M.-C.; McGehee, M. D.; Sun, X.; Dai, H. Solar-Driven, Highly Sustained Splitting of Seawater into Hydrogen and Oxygen Fuels. *Proc. Natl. Acad. Sci.* **2019**, *116* (14), 6624–6629.

(23) Cox, C. R.; Lee, J. Z.; Nocera, D. G.; Buonassisi, T. Ten-Percent Solar-to-Fuel Conversion with Nonprecious Materials. *Proc. Natl. Acad. Sci.* **2014**, *111* (39), 14057–14061.

(24) Li, J.; Wang, Y.; Zhou, T.; Zhang, H.; Sun, X.; Tang, J.; Zhang, L.; Al-Enizi, A. M.; Yang, Z.; Zheng, G. Nanoparticle Superlattices as Efficient Bifunctional Electrocatalysts for Water Splitting. *J. Am. Chem. Soc.* **2015**, *137* (45), 14305–14312.

(25) Landman, A.; Dotan, H.; Shter, G. E.; Wullenkord, M.; Houaijia, A.; Maljusch, A.; Grader, G. S.; Rothschild, A. Photoelectrochemical Water Splitting in Separate Oxygen and Hydrogen Cells. *Nat. Mater.* **2017**, *16* (6), 646–651.

(26) Park, H.; Park, I. J.; Lee, M. G.; Kwon, K. C.; Hong, S.-P.; Kim, D. H.; Lee, S. A.; Lee, T. H.; Kim, C.; Moon, C. W.; Son, D.-Y.; Jung, G. H.; Yang, H. S.; Lee, J. R.; Lee, J.; Park, N.-G.; Kim, S. Y.; Kim, J. Y.; Jang, H. W. Water Splitting Exceeding 17% Solar-to-Hydrogen

Conversion Efficiency Using Solution-Processed Ni-Based Electrocatalysts and Perovskite/Si Tandem Solar Cell. *ACS Appl. Mater. Interfaces* **2019**, *11* (37), 33835–33843.

(27) Chen, H.; Song, L.; Ouyang, S.; Wang, J.; Lv, J.; Ye, J. Co and Fe Codoped $WO_{2.72}$ as Alkaline-Solution-Available Oxygen Evolution Reaction Catalyst to Construct Photovoltaic Water Splitting System with Solar-To-Hydrogen Efficiency of 16.9. *Adv. Sci.* **2019**, *6* (16), 1900465.

(28) Lee, M.; Turan, B.; Becker, J.-P.; Welter, K.; Klingebiel, B.; Neumann, E.; Sohn, Y. J.; Merdzhanova, T.; Kirchartz, T.; Finger, F.; Rau, U.; Haas, S. A Bias‐Free, Stand‐Alone, and Scalable Photovoltaic–Electrochemical Device for Solar Hydrogen Production. *Adv. Sustainable Syst.* **2020**, *4* (8), 2000070.

(29) Luo, J.; Im, J.-H.; Mayer, M. T.; Schreier, M.; Nazeeruddin, M. K.; Park, N.-G.; Tilley, S. D.; Fan, H. J.; Gratzel, M. Water Photolysis at 12.3% Efficiency via Perovskite Photovoltaics and Earth-Abundant Catalysts. *Science* **2014**, *345* (6204), 1593–1596.

(30) Esiner, S.; van Eersel, H.; Wienk, M. M.; Janssen, R. A. J. Triple Junction Polymer Solar Cells for Photoelectrochemical Water Splitting. *Adv. Mater.* **2013**, *25* (21), 2932–2936.

(31) Esiner, S.; Willems, R. E. M.; Furlan, A.; Li, W.; Wienk, M. M.; Janssen, R. A. J. Photoelectrochemical Water Splitting in an Organic Artificial Leaf. *J. Mater. Chem. A* **2015**, *3* (47), 23936–23945.

(32) Esiner, S.; van Eersel, H.; van Pruissen, G. W. P.; Turbiez, M.; Wienk, M. M.; Janssen, R. A. J. Water Splitting with Series-Connected Polymer Solar Cells. *ACS Appl. Mater. Interfaces* **2016**, *8* (40), 26972–26981.

(33) Esiner, S.; van Pruissen, G. W. P.; Wienk, M. M.; Janssen, R. A. J. Optimized Light-Driven Electrochemical Water Splitting with Tandem Polymer Solar Cells. *J. Mater. Chem. A* **2016**, *4* (14), 5107–5114.

(34) Li, Z.; Wu, S.; Zhang, J.; Lee, K. C.; Lei, H.; Lin, F.; Wang, Z.; Zhu, Z.; Jen A. K. Y. Hybrid Perovskite‐Organic Flexible Tandem Solar Cell Enabling Highly Efficient Electrocatalysis Overall Water Splitting. *Adv. Energy Mater.* **2020**, *10* (18), 2000361.

(35) Peharz, G.; Dimroth, F.; Wittstadt, U. Solar Hydrogen Production by Water Splitting with a Conversion Efficiency of 18%.. *J. Hydrogen Energy* **2007**, *32* (15), 3248–3252.

(36) Fujii, K.; Nakamura, S.; Sugiyama, M.; Watanabe, K.; Bagheri, B.; Nakano, Y. Characteristics of Hydrogen Generation from Water Splitting by Polymer Electrolyte Electrochemical Cell Directly Connected with Concentrated Photovoltaic Cell. . *J. Hydrogen Energy* **2013**, *38* (34), 14424–14432.

(37) Nakamura, A.; Ota, Y.; Koike, K.; Hidaka, Y.; Nishioka, K.; Sugiyama, M.; Fujii, K. A 24.4% Solar to Hydrogen Energy Conversion Efficiency by Combining Concentrator Photovoltaic Modules and Electrochemical Cells. *Appl. Phys. Express* **2015**, *8* (10), 107101.

(38) Jia, J.; Seitz, L. C.; Benck, J. D.; Huo, Y.; Chen, Y.; Ng, J. W. D.; Bilir, T.; Harris, J. S.; Jaramillo, T. F. Solar Water Splitting by Photovoltaic-Electrolysis with a Solar-to-Hydrogen Efficiency over 30%. *Nat. Commun*. **2016**, *7* (1). 13237.

(39) Hsu, S.-H.; Miao, J.; Zhang, L.; Gao, J.; Wang, H.; Tao, H.; Hung, S.-F.; Vasileff, A.; Qiao, S. Z.; Liu, B. An Earth-Abundant Catalyst-Based Seawater Photoelectrolysis System with 17.9% Solar-to-Hydrogen Efficiency. *Adv. Mater.* **2018**, *30* (18), 1707261.

(40) Elias, X.; Liu, Q.; Gimbert-Suriñach, C.; Matheu, R.; Mantilla-Perez, P.; Martinez-Otero, A.; Sala, X.; Martorell, J.; Llobet, A. Neutral Water Splitting Catalysis with a High FF Triple Junction Polymer Cell. *ACS Catal.* **2016**, *6* (5), 3310–3316.

(41) Liu, J.; Liu, Y.; Liu, N.; Han, Y.; Zhang, X.; Huang, H.; Lifshitz, Y.; Lee, S.-T.; Zhong, J.; Kang, Z. Metal-free Efficient Photocatalyst for Stable Visible Water Splitting Via a Two-electron Pathway. *Science* **2015**, *347* (6225), 970–974.

(42) Kosar, S.; Pihosh, Y.; Turkevych, I.; Mawatari, K.; Uemura, J.; Kazoe, Y.; Makita, K.; Sugaya, T.; Matsui, t.; Fujita, D.; Tosa, M.; Struk, Y. M.; Kondo, M.; Kitamori, T. Tandem Photovoltaic–photoelectrochemical GaAs/InGaAsP–WO_3/$BiVO_4$ Device for Solar Hydrogen Generation. *Jpn. J. Appl. Phys.* **2016**, *55*, 04ES01.

(43) Matheu, R.; Ertem, M. Z.; Benet-Buchholz, J.; Coronado, E.; Batista, V. S.; Sala, X.; Llobet, A. Intramolecular Proton Transfer Boosts Water Oxidation Catalyzed by a Ru Complex. *J. Am. Chem. Soc.* **2015**, *137* (33), 10786–10795.

(44) Creus, J.; Matheu, R.; Peñafiel, I.; Moonshiram, D.; Blondeau, P.; Benet-Buchholz, J.; García-Antón, J.; Sala, X.; Godard, C.; Llobet, A. A Million Turnover Molecular Anode for Catalytic Water Oxidation. *Angew. Chem.- Int. Ed.* **2016**, *55* (49), 15382–15386.

(45) Xu, J.; Murphy, S.; Xiong, D.; Cai, R.; Wei, X.-K.; Heggen, M.; Barborini, E.; Vinati, S.; Dunin-Borkowski, R. E.; Palmer, R. E.; Liu, L. Cluster Beam Deposition of Ultrafine Cobalt and Ruthenium Clusters for Efficient and Stable Oxygen Evolution Reaction. *ACS Appl. Energy Mater.* **2018**, *1* (7), 3013–3018.

(46) Hoque, M. A.; Gil-Sepulcre, M.; de Aguirre, A.; Elemans, J. A. A. W.; Moonshiram, D.; Matheu, R.; Shi, Y.; Benet-Buchholz, J.; Sala, X.; Malfois, M.; Solano, E.; Lim, J.; Manjón, A.; Scheu, C.; Lanza, M.; Maseras, F.; Gimbert-Suriñach C.; Llobet, A. Water Oxidation Electroncatalysis using ruthenium coordination oligomers adsorbed on multiwalled carbon nanotubes. *Nat. Chem.* **2020**, DOI: 10.1038/s41557-020-0548-7.

(47) Matheu, R.; Moreno-Hernandez, I. A.; Sala, X.; Gray, H. B.; Brunschwig, B. S.; Llobet, A.; Lewis, N. S. Photoelectrochemical Behavior of a Molecular Ru-Based Water-Oxidation Catalyst Bound to TiO2-Protected Si Photoanodes. *J. Am. Chem. Soc.* **2017**, *139* (33), 11345–11348.

(48) Grau, S.; Berardi, S.; Moya, A.; Matheu, R.; Cristino, V.; Vilatela, J. J.; Bignozzi, C. A.; Caramori, S.; Gimbert-Suriñach, C.; Llobet, A. A Hybrid Molecular Photoanode for Efficient Light-Induced Water Oxidation. *Sustain. Energy Fuels* **2018**, *2* (9), 1979–1985.

(49) Garrido-Barros, P.; Matheu, R.; Gimbert-Suriñach, C.; Llobet, A. Electronic, Mechanistic, and Structural Factors That Influence the Performance of Molecular Water Oxidation Catalysts Anchored on Electrode Surfaces. *Curr. Opin Electrochem.* **2019**, *15*, 140–147.

(50) Tsuji, E.; Imanishi, A.; Fukui, K.; Nakato, Y. Electrocatalytic Activity of Amorphous RuO2 Electrode for Oxygen Evolution in an Aqueous Solution. *Electrochimica Acta* **2011**, *56* (5), 2009–2016.

(51) Spurgeon, J. M.; Velazquez, J. M.; McDowell, M. T. Improving O2 Production of WO3 Photoanodes with IrO2 in Acidic Aqueous Electrolyte. *Phys. Chem. Chem. Phys.* **2014**, *16* (8), 3623.

(52) Yang, W. S.; Park, B.-W.; Jung, E. H.; Jeon, N. J.; Kim, Y. C.; Lee, D. U.; Shin, S. S.; Seo, J.; Kim, E. K.; Noh, J. H.; Seok, S. I. Iodide Management in Formamidinium-Lead-Halide–Based Perovskite Layers for Efficient Solar Cells. *Science* **2017**, *356* (6345), 1376–1379.

(53) Gelmetti, I.; Montcada, N. F.; Pérez-Rodríguez, A.; Barrena, E.; Ocal, C.; García-Benito, I.; Molina-Ontoria, A.; Martín, N.; Vidal-Ferran, A.; Palomares, E. Energy Alignment and Recombination in Perovskite Solar Cells: Weighted Influence on the Open Circuit Voltage. *Energy Environ. Sci.* **2019**, *12* (4), 1309–1316.

(54) Matheu, R.; Garrido-Barros, P.; Gil-Sepulcre, M.; Ertem, M. Z.; Sala, X.; Gimbert-Suriñach, C.; Llobet, A. The Development of Molecular Water Oxidation Catalysts. *Nat. Rev. Chem.* **2019**, *3* (5), 331–341.

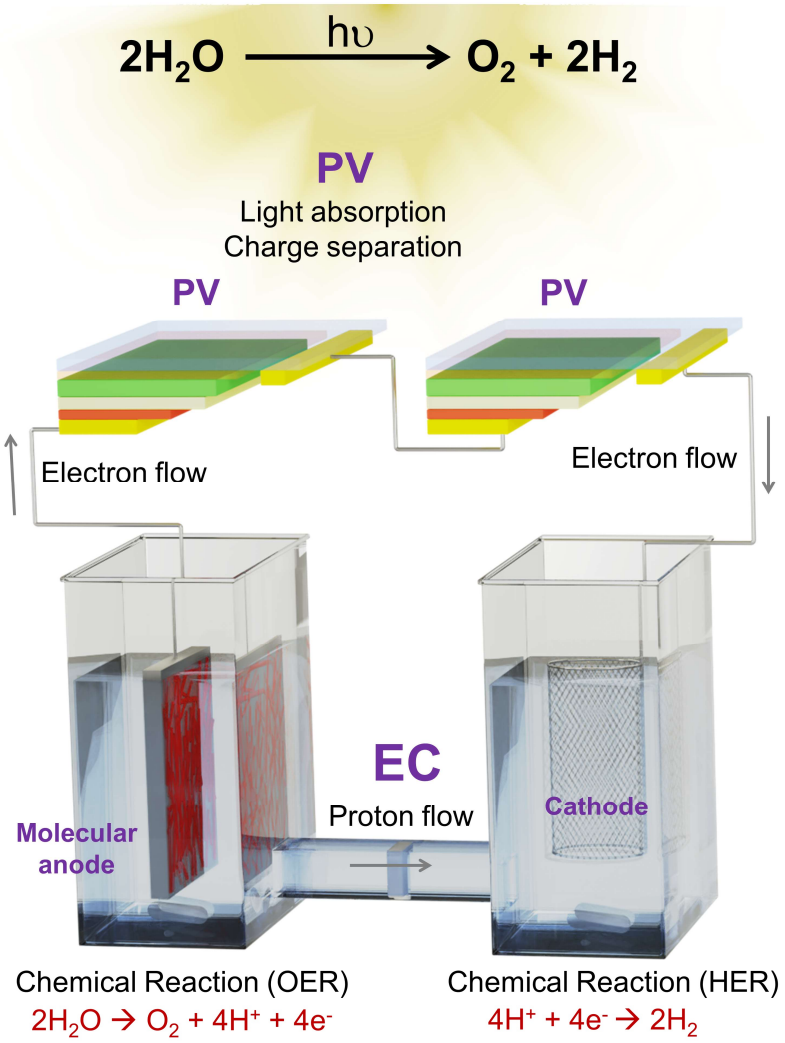

Figure 1. Schematic of one of the PV-EC devices built in this work for light induced water splitting. PV = perovskite solar cell; A = molecular anode for the oxygen evolution reaction (OER); C = platinum mesh cathode for the hydrogen evolution reaction (HER). The electrolyte solution is pH 7 phosphate buffer and the two compartments are separated by a frit.

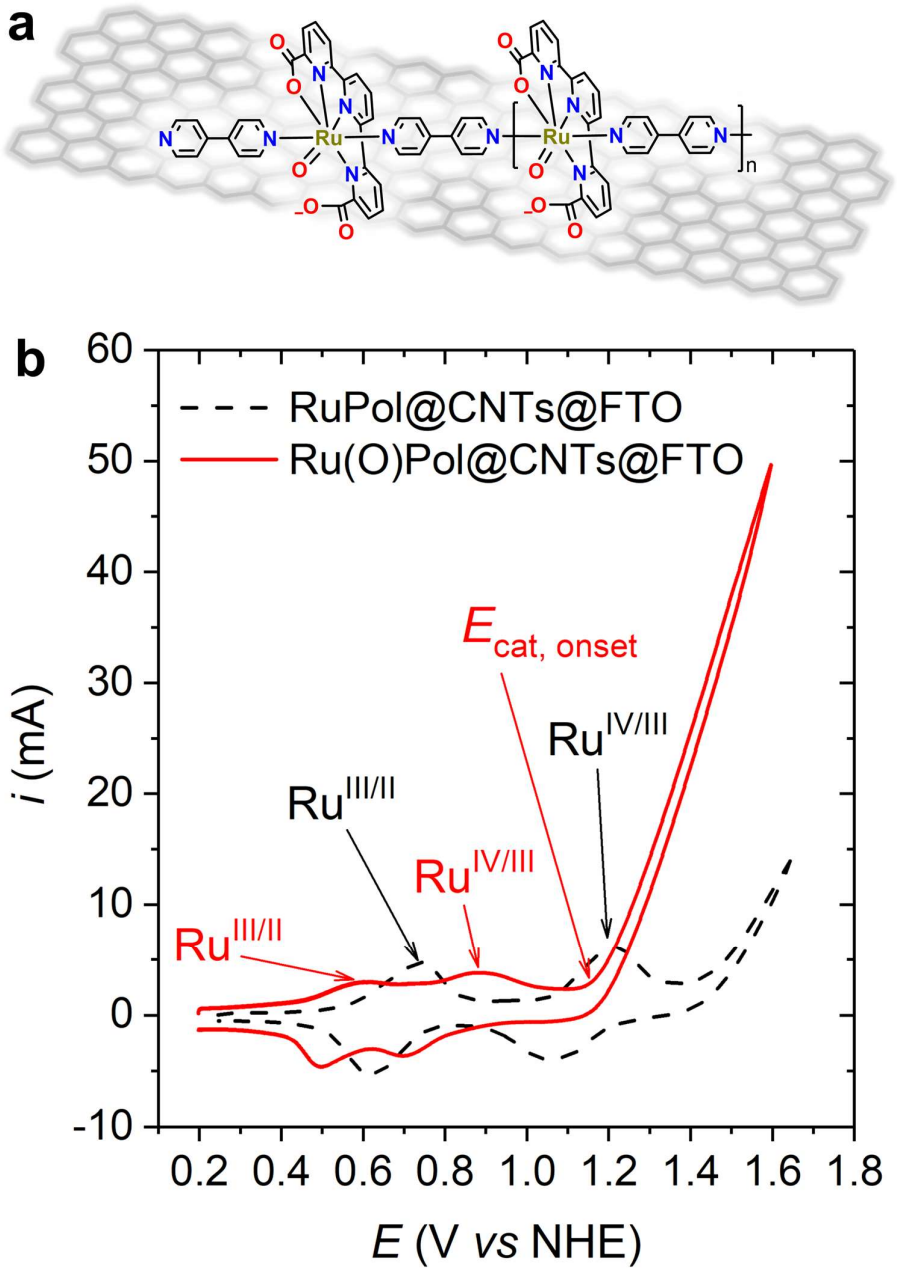

Figure 2. The oligomeric molecular anode before (RuPol@CNTs@FTO) and after (Ru(O)Pol@CNTs@FTO) activation. a) illustration of the architecture of the active Ru(O)Pol catalyst anchored on CNT. b) cyclic voltammetry of RuPol@CNTs@FTO (dashed black trace) and Ru(O)Pol@CNTs@FTO (red solid trace) as working electrodes at pH 7 phosphate buffer with an ionic strength of 1 M. The counter and reference electrodes are Pt mesh and Hg/Hg_2SO_4 (saturated K_2SO_4), respectively.

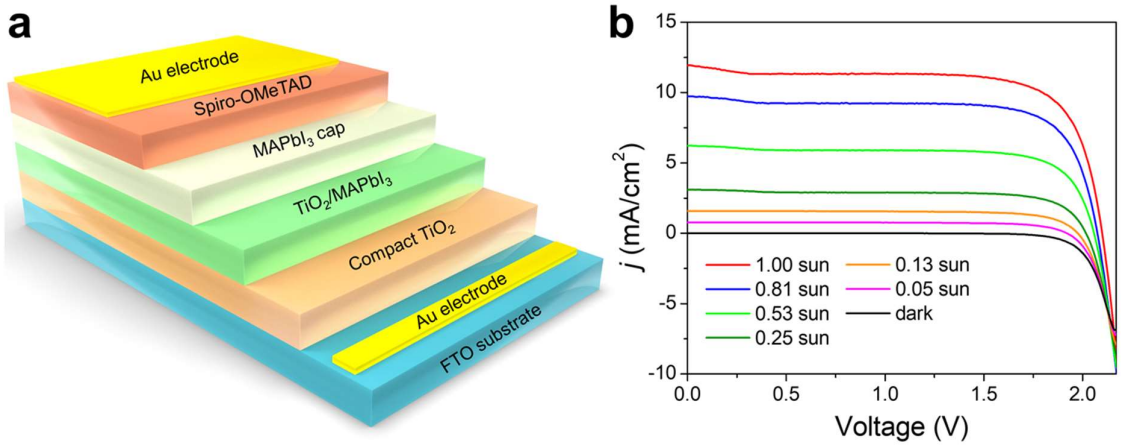

Figure 3. The performance of two lab-fabricated perovskite solar cells connected in series. a) schematic representation of a single perovskite solar cell configuration. b) the *J-V* characteristics of two series-connected perovskite solar cells under the illumination at different light intensities and in the dark.

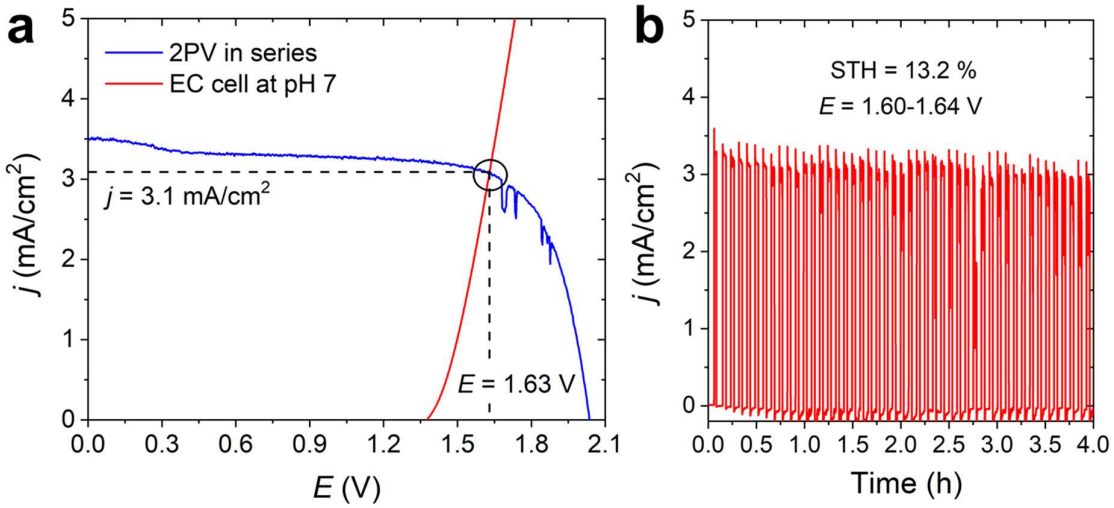

Figure 4. PV-EC water splitting device based on two lab-fabricated perovskite solar cells and the Ru(O)Pol@CNTs@FTO anode. a) plot of *J-V* curves of the two perovskite solar cells (2PV) connected in series, under simulated illumination (blue), and the electrolyzer (EC) composed of Ru(O)Pol@CNTs@FTO molecular anode and Pt mesh cathode in a two-electrode configuration at pH 7 (red). The overlapping point indicates the expected operating voltage and current density of the PV-EC water splitting. The effective illuminated surface area of the perovskite cells is 0.18 cm^2, and the geometric size of the anode is 1.87 cm^2. b) Photocurrent density *vs*. time plot of the PV-EC water splitting device under chopped light illumination at pH 7.

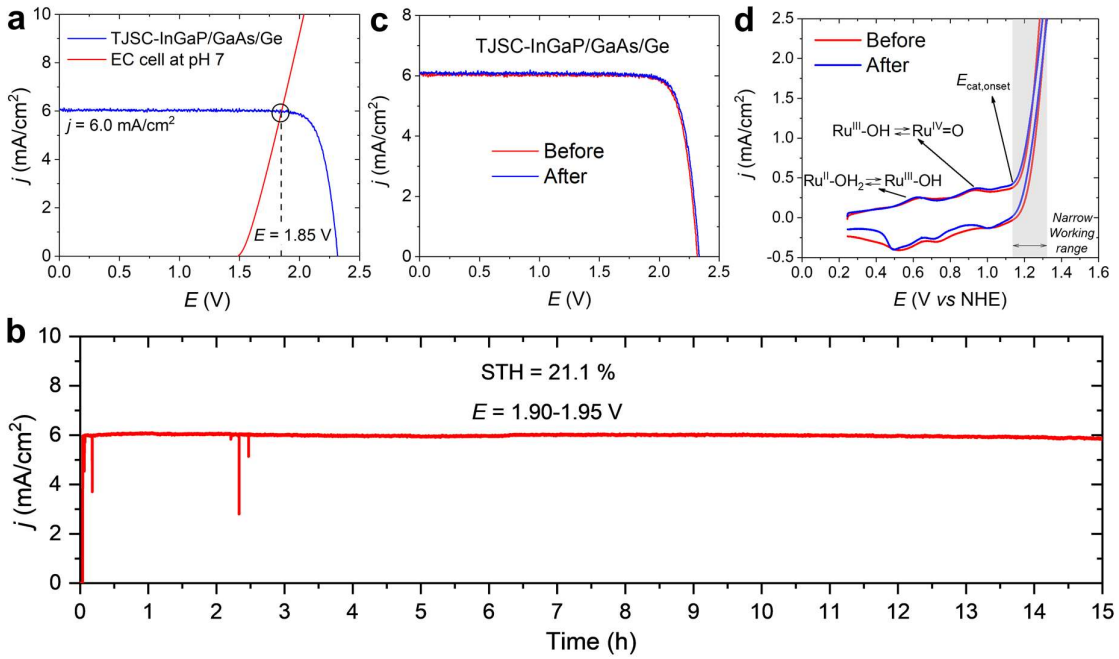

Figure 5. PV-EC water splitting device based on commercially available TJSC-InGaP/GaAs/Ge solar cell and the Ru(O)Pol@CNTs@FTO anode. a) plot of *J-V* curve for the triple junction InGaP/GaAs/Ge solar cell under illumination, and linear sweep voltammetry of the electrolyzer using an Ru(O)Pol@CNTs@FTO electrode as anode and a Pt mesh as cathode in a two-electrode configuration. The effective illuminated surface area of this solar cell is 0.18 cm^2, and the geometric size of the anode is 1.8 cm^2. b) photocurrent density *vs.* time plot of a PV-EC experiment under illumination at pH 7. c) Plot of *J-V* for the TJSC-InGaP/GaAs/Ge and, d) the Ru(O)Pol@CNTs@FTO molecular electrode before and after >15 hours continuous water splitting using the PV-EC device.